APPLICATION OF NON-LINEAR EDDY-VISCOSITY AND DIFFERENTIAL STRESS CLOSURES TO SEPARATED FLOW

David D. Apsley

and

Michael A. Leschziner
Department of Mechanical Engineering, UMIST
Manchester, M60 1QD, England

ABSTRACT

Non-linear eddy-viscosity models and second-moment closure are examined, both theoretically and by comparison with 2-d and 3-d test cases featuring separation from mildly curved surfaces. It is found that, whereas non-linear stress-strain relations improve the prediction of normal-stress anisotropy, the mean flow dynamics are primarily influenced by the shear stress and, in particular, by the use of a strain-dependent linear coefficient. The advantages of second-moment closure are most apparent in fully 3-d flows, where several stress components are important. Determination of the turbulent length scale remains a crucial element in the performance of models in non-equilibrium flows.

INTRODUCTION

Practical flows demand the application of turbulence models which have, almost invariably, been calibrated by reference to simple shear. This extrapolation can only be successful if the models account for all essential physical mechanisms that play a role in highly non-equilibrium conditions.

The set of second-moment transport equations form a sound modelling framework for flows involving complex strain, mainly because the influential production terms do not require approximation. However, their performance is sensitive to the modelling of stress redistribution. Non-linear eddy-viscosity models (NLEVMs) represent, potentially, an alternative to second-moment closure. However, since these models contain much less of the physics that are explicitly accounted for in the second-moment equations, NLEVMs require both very careful calibration and evaluation over a broad range of non-equilibrium conditions.

Among the many non-equilibrium flow phenomena encountered in practice, separation from curved surfaces is especially challenging. Specifically, the location of separation is highly sensitive to the complex interplay between the boundary layer approaching separation, including the semi-viscous near-wall region, surface curvature and the adverse pressure gradient. The important role of the near-wall region makes it desirable to employ models which have been designed and calibrated for use right through the viscous sublayer.

This paper examines the performance of four differential stress models (DSMs) and three NLEVMs in 2-d and 3-d flows in which separation from flat or gently-curving surfaces is provoked by an adverse pressure gradient.

TURBULENCE MODELS

Second-Order Closure

Second-moment closure refers to the modelling and solution of differential transport equations of the form

$$\rho\frac{D}{Dt}(\overline{u_i u_j}) = P_{ij} + \Phi_{ij} + \frac{\partial}{\partial x_k} d_{ijk} - \rho\varepsilon_{ij} \quad ,$$

where the advection and production (P_{ij}) terms are exact, and the pressure-strain correlation (Φ_{ij}), diffusion (d_{ijk}) and dissipation (ε_{ij}) terms require modelling. The models considered here are those of Gibson and Launder (1978), Speziale *et al.* (1991), Shima (1998) and Jakirlic and Hanjalic (1995). The first applies to high-*Re* conditions only and is used here as a datum. The novelty of the second is a quadratic pressure-strain approximation for the slow and rapid parts of the pressure-strain correlation,

$$\mathbf{\Phi}^{(1)} = -\varepsilon[c_1\mathbf{a} + c_1'(\mathbf{a}^2 - \tfrac{1}{3}\{\mathbf{a}^2\}\mathbf{I})] ,$$

$$\mathbf{\Phi}^{(2)} = \varepsilon[c_{21}\mathbf{s} + c_{22}(\mathbf{sa} + \mathbf{as} - \tfrac{2}{3}\{\mathbf{as}\}\mathbf{I}) + c_{23}(\boldsymbol{\omega}\mathbf{a} - \mathbf{a}\boldsymbol{\omega}) + c_{24}\{\mathbf{as}\}\mathbf{a}] ,$$

which, reportedly, obviates the need for explicit wall-proximity corrections. Here, $a_{ij} = \overline{u_i u_j}/k - \frac{2}{3}\delta_{ij}$ is the anisotropy tensor, whilst $s_{ij} = \frac{1}{2}(U_{i,j} + U_{j,i})k/\varepsilon$ and $\omega_{ij} = \frac{1}{2}(U_{i,j} - U_{j,i})k/\varepsilon$ are the non-dimensional mean strain and vorticity tensors, respectively. For brevity, a second-rank tensor is denoted by bold type and its trace by $\{.\}$. The other models use wall corrections and simple "return-to-isotropy" (c_1'=0) and "isotropisation-of-production" ($c_{22} = c_{23} = \frac{3}{4}c_{21}$, $c_{24} = 0$) pressure-strain approximations - except for Shima's rapid term, which is linear. The last two models are true low-*Re* closures, with coefficients which are functions of the turbulence Reynolds number $R_t \equiv k^2/\nu\varepsilon$ and the anisotropy invariants $a_2 \equiv \{\mathbf{a}^2\}$ and $a_3 \equiv \{\mathbf{a}^3\}$, together with Lumley's flatness parameter $A \equiv 1 - \frac{9}{8}(a_2 - a_3)$, which takes the values 0 and 1 in 2-d and isotropic turbulence, respectively. Jakirlic and Hanjalic's model explicitly employs an anisotropic dissipation of the form

$$\boldsymbol{\varepsilon} = f_\varepsilon \tfrac{2}{3}\mathbf{I} + (1 - f_\varepsilon)\boldsymbol{\varepsilon}^* ,$$

where $\boldsymbol{\varepsilon}^*$ has the correct asymptotic behaviour and $f_\varepsilon \to 0$ as solid boundaries are approached. An additional flatness parameter is constructed from $\boldsymbol{\varepsilon}$. For other models, any anisotropic dissipation is assumed to be absorbed within the pressure-strain model. For the Jakirlic and Hanjalic model we have examined the additional source term proposed by Hanjalic *et al.* (1997) in the ε equation:

$$S_l = \max[(\gamma^2 - 1)\gamma^2, 0]\frac{\tilde{\varepsilon}\varepsilon}{k}A , \qquad \gamma = \left|\nabla\left(\frac{k^{3/2}}{2.5\varepsilon}\right)\right| .$$

This term, which is determined by the gradient of the dissipation length, is designed to prevent excessive growth of the turbulent length scale in flows with large irrotational strains (those which contribute to the production of turbulence energy, k).

Non-Linear Eddy-Viscosity Models

NLEVMs consist of two elements: a non-dimensional constitutive relation between anisotropy $\mathbf{a}$ and irrotational/rotational strains ($\mathbf{s}$,$\boldsymbol{\omega}$) and transport equations for turbulence scalars (*e.g.* k and ε) to determine k. The Cayleigh-Hamilton theorem dictates that there are only 10 tensorially-independent, symmetric, traceless, polynomial combinations of $\mathbf{s}$ and $\boldsymbol{\omega}$, so that, with a particular basis (the choice of which will be discussed below), the general non-linear stress-strain relationship may be written:

$$\begin{aligned}\mathbf{a} = &-2c_1\mathbf{s} \\ &+c_2(\mathbf{s}^2 - \tfrac{1}{3}\{\mathbf{s}^2\}\mathbf{I}) + c_3(\boldsymbol{\omega}\mathbf{s} - \mathbf{s}\boldsymbol{\omega}) + c_4(\boldsymbol{\omega}^2 - \tfrac{1}{3}\{\boldsymbol{\omega}^2\}\mathbf{I}) \\ &+c_5(\boldsymbol{\omega}^2\mathbf{s} + \mathbf{s}\boldsymbol{\omega}^2 - \{\boldsymbol{\omega}^2\}\mathbf{s} - \tfrac{2}{3}\{\boldsymbol{\omega}\mathbf{s}\boldsymbol{\omega}\}\mathbf{I}) + c_6(\boldsymbol{\omega}\mathbf{s}^2 - \mathbf{s}^2\boldsymbol{\omega}) \\ &+c_7[\boldsymbol{\omega}^2\mathbf{s}^2 + \mathbf{s}^2\boldsymbol{\omega}^2 - \{\boldsymbol{\omega}^2\}(\mathbf{s}^2 - \tfrac{1}{3}\{\mathbf{s}^2\}\mathbf{I}) - \tfrac{2}{3}\{\mathbf{s}^2\boldsymbol{\omega}^2\}\mathbf{I}] \\ &+c_8[\mathbf{s}^2\boldsymbol{\omega}\mathbf{s} - \mathbf{s}\boldsymbol{\omega}\mathbf{s}^2 - \tfrac{1}{2}\{\mathbf{s}^2\}(\boldsymbol{\omega}\mathbf{s} - \mathbf{s}\boldsymbol{\omega})] \\ &+c_9[\boldsymbol{\omega}\mathbf{s}\boldsymbol{\omega}^2 - \boldsymbol{\omega}^2\mathbf{s}\boldsymbol{\omega} - \tfrac{1}{2}\{\boldsymbol{\omega}^2\}(\boldsymbol{\omega}\mathbf{s} - \mathbf{s}\boldsymbol{\omega})] \\ &+c_{10}(\boldsymbol{\omega}\mathbf{s}^2\boldsymbol{\omega}^2 - \boldsymbol{\omega}^2\mathbf{s}^2\boldsymbol{\omega})\end{aligned}$$

where successive lines contain tensor bases of increasing degree in $\boldsymbol{\omega}$ and $\mathbf{s}$, and the c_i are functions of the irreducible invariants $\{\mathbf{s}^2\}$, $\{\boldsymbol{\omega}^2\}$, $\{\mathbf{s}^3\}$, $\{\mathbf{s}\boldsymbol{\omega}^2\}$, and $\{\mathbf{s}^2\boldsymbol{\omega}^2\}$. In 2-d incompressible flow, one finds that

$$\mathbf{s}^2 = (s_{11}^2 + s_{12}^2)\mathbf{I}_2 = \tfrac{1}{2}\{\mathbf{s}^2\}\mathbf{I}_2 ,$$

$$\boldsymbol{\omega}^2 = -\omega_{12}^2\mathbf{I}_2 = \tfrac{1}{2}\{\boldsymbol{\omega}^2\}\mathbf{I}_2 ,$$

where $\mathbf{I}_2$=diag(1,1,0), so that, with the (slightly complex) bases chosen here, the cubic and higher-degree terms vanish. *A quadratic model, therefore, is sufficient to compute a 2-d flow*. Terms of higher degree only become necessary in 3-d flows. An alternative view is to note that the symmetric, traceless anisotropy tensor has only 3 and 5 independent components in 2- and 3-d flows, respectively. Sufficient degrees of freedom (*i.e.* non-zero c_i) are then met at quadratic and cubic levels in the two cases. Indeed, if one adheres to the principle that pure rotation generates no anisotropy, then c_4=0, and a cubic model (c_1,...,c_6) has precisely the correct number of degrees of freedom. *A cubic model, therefore, is deemed appropriate for general 3-d flows*. The coefficients of three stress-strain relationships that we have investigated - Gatski and Speziale (1993), Craft *et al.* (1996), Apsley and Leschziner (1998) - are given in the Appendix. The first is quadratic and high-*Re*; the last two are cubic and low-*Re*.

The linear term corresponds to the standard k-ε model, with $c_1 = c_\mu$. For simple shear, the linear term makes no contribution to the normal stresses, but the quadratic terms give

$$a_{11} = \tfrac{1}{12}(c_2 + 6c_3 - c_4)\sigma^2 ,$$

$$a_{22} = \tfrac{1}{12}(c_2 - 6c_3 - c_4)\sigma^2 ,$$

where $\sigma = (k/\varepsilon)(\partial U/\partial y)$, and are responsible for normal-stress anisotropy. The Craft *et al.* model includes a term proportional to $(s_{ij}s_{ij} - \omega_{ij}\omega_{ij})\mathbf{s}$, which is herein regarded as part of the linear term. In curved shear flow,

$$s_{ij}s_{ij} - \omega_{ij}\omega_{ij} = -2\frac{\partial U}{\partial R}\frac{U}{R}\left(\frac{k}{\varepsilon}\right)^2 ,$$

where R is the radius of curvature. This component, therefore, yields sensitivity to mean streamline curvature.

TEST CASE COMPARISONS

We report solutions for an asymmetric plane diffuser (Obi *et al.*, 1993), axisymmetric transonic bump (Bachalo

and Johnson, 1986) and a 3-d wing-body junction (Fleming *et al.*, 1993), all shown in Figure 1. Calculations were performed with a general-purpose, multi-block, non-orthogonal, finite-volume procedure, using collocated variable storage and the SIMPLE pressure-correction algorithm. All transport equations were discretised with a second-order, upwind-biased advection scheme.

Asymmetric Plane Diffuser (Obi *et al.*, 1993)

This nominally 2-d geometry has one plane and one inclined wall and diffuses the flow from H to $4.7H$ over distance $21H$. The flow separates from the angled wall at $x/H \approx 11$, due to the adverse pressure gradient, and reattaches at $x/H \approx 26$. A mesh of 292×96 cells was used for low-*Re* calculations. For high-*Re* models, cells within 5% local channel height of the walls were amalgamated to form the wall-law region. Fully-developed channel-flow calculations at $Re=21200$ were used to prescribe inflow profiles at $x/H=-11$.

Figures 2 and 3 show mean-velocity profiles in the diffusing section for NLEVMs and DSMs, respectively. With the exception of the Jakirlic and Hanjalic (1995) DSM, all advanced closures returned clear improvements over the baseline linear k-ε model, predicting separation and cross-channel asymmetry. The length-scale correction of Hanjalic *et al.* (1997) had no significant effect here. Greater reversed-flow velocities with high-*Re* models suggest that, despite their other defects (including lack of smoothness near the wall, due to the size of the near-wall cell), wall-function treatments often control near-wall length scales better than current low-*Re* closures. Differences between predictions with the Speziale *et al.* (1991) and Gibson and Launder (1978) models primarily arise from the different ε-equation constant - $C_{\varepsilon 1}=1.83$ as opposed to 1.92 - rather than the pressure-strain approximations. Figure 4 shows shear-stress predictions. The DSMs correctly predict enhanced levels in the upper half of the channel, but, whereas experiment reveals steady growth along the channel, computations exaggerate this significantly in the first half of the diffuser.

Figure 5 distinguishes the effect of the non-linear terms in the Craft *et al.* model. The Figure demonstrates that: (a) the improved mean-flow profiles are primarily attributable to a strain-dependent C_μ, rather than a non-linear stress-strain relationship; (b) addition of quadratic terms greatly improves the prediction of anisotropy - particularly the streamwise component - and promotes slightly earlier separation, perhaps due to reduction in the wall-normal stress (the quadratic terms have no direct effect on the generation of turbulence energy in 2-d flows); (c) the curvature-dependent term has negligible influence here.

Axisymmetric Transonic Bump (Bachalo and Johnson, 1986)

The transonic flow over a circular-arc bump (chord c) gives rise to separation just downstream of a shock at $x/c=0.66$ for a free-stream Mach number of 0.875. Low-Re calculations were performed with a mesh of 220×100 control volumes and wall-function calculations by amalgamating the 21 cells nearest the surface. Plug flow was assumed at $x/c=-4.0$, to give the correct upstream boundary-layer height.

Figures 6 and 7 show the C_p distribution over the bump for NLEVMs and DSMs respectively. All the advanced models predict earlier shocks and separation than the standard k-ε model. However, the mean-velocity profiles in Figure 8 show the advanced closures to predict too much recirculation. All models tested yield insufficient rate of recovery in the wake region.

Wing-Body Junction (Fleming *et al.*, 1993)

This 3-d junction flow is formed by a symmetric aerofoil (3:2 semi-elliptic nose and NACA 0020 tail) affixed normally to a flat plate. The Reynolds number based on aerofoil thickness T is 115000 and the chord:thickness ratio c/T is 4.25. The flow is dominated by the characteristic "horseshoe" vortex. The flow was computed with a single-block, low-*Re* mesh of 144×48×48 control volumes, assuming symmetry in the wing centre-plane. For high-*Re* models, cells close to the walls were amalgamated to form a 144×36×36-control-volume mesh. Inflow profiles were based on the experimental data at $x/T=-18$.

Figure 9 shows C_P distributions on the wing for representative linear and non-linear EVMs and differential stress closure. The pressure distribution is almost model-independent and shows that, whereas the pressure near the plane surface is well-predicted, in the more 2-d region the wing pressure minimum is underestimated and displaced forward with respect to experiment. The pressure distribution is insensitive to the near-wall treatment.

Figure 10 shows the mean velocity in the upstream vortex and Figure 11 the secondary-flow velocity in a crosswind plane. Second-order closures predict stronger, but less extensive, vortex structures than both linear and non-linear eddy-viscosity models in this highly three-dimensional flow.

CONCLUSIONS

Theoretical considerations suggest that a cubic stress-strain relationship is required for first-order closures to represent anisotropy in general 3-d flows. In practice, however, the performance of such models is primarily influenced by the variation in the linear term, for which C_μ should decay at least as fast as the reciprocal of the non-dimensional strain rate for large velocity gradients.

In the chosen test cases, second-moment closures produced results comparable to NLEVMs for 2-d flows, but were significantly better for 3-d flows, where the number of dynamically-important stress components is greater. Results showed variation attributable to length-scale modelling. The difference between high-*Re* models, for example, could be seen to depend on $C_{\varepsilon 2}$, and, in the diffuser case, wall-function calculations gave better results in adverse pressure gradients than models which integrated through the viscous sublayer.

ACKNOWLEDGEMENT

The authors gratefully acknowledge the financial support provided by the UK Engineering and Physical Sciences Research Council (EPSRC), British Aerospace plc, Rolls-Royce plc and the UK Defence Evaluation and Research Agency (DERA). Thanks are also due to Dr. A.Gould of BAe (SRC) for many useful discussions.

APPENDIX: COEFFICIENTS IN NON-LINEAR STRESS-STRAIN RELATIONSHIPS

Gatski and Speziale (1993) - as regularised by Speziale and Xu (1996):

$$c_1 = \frac{(1+2\zeta^2)(1+6\eta^5)+\frac{5}{3}\eta^2}{(1+2\zeta^2)(1+2\zeta^2+\eta^2+6\beta_1\eta^6)}\left(\frac{\alpha_1}{2}\right),$$

$$c_{2,3} = \frac{(1+2\zeta^2)(1+\eta^4)+\frac{2}{3}\eta^2}{(1+2\zeta^2)(1+2\zeta^2+\beta_{3,2}\eta^6)}\alpha_{3,2} \quad ,$$

$$\eta = \tfrac{1}{2}(\alpha_3/\alpha_1)(s_{ij}s_{ij})^{1/2}, \quad \zeta = (\alpha_2/\alpha_1)(\omega_{ij}\omega_{ij})^{1/2},$$

$$\alpha_1 = 0.227, \quad \alpha_2 = 0.0424, \quad \alpha_3 = 0.0397,$$

$$\beta_1 = 7.0, \quad \beta_2 = 6.3, \quad \beta_3 = 4.0 \quad .$$

Craft, Launder and Suga (1996):

$$c_1 = c_\mu f_\mu[1+10c_\mu^2(\tilde{s}^2-\overline{\omega}^2)] \ ,$$

$$(c_2\ ,\ c_3\ ,\ c_4) = (-0.4\ ,\ 0.4\ ,\ -1.04)\ c_\mu f_\mu \ , \qquad c_6 = 80c_\mu^3 f_\mu$$

$$c_\mu = \frac{0.3(1-\exp(-0.36e^{0.75\tilde{s}}))}{1+0.35\tilde{s}^{3/2}},$$

$$f_\mu = 1-\exp[-(R_t/90)^{1/2}-(R_t/400)^2],$$

$$\overline{s} = (2s_{ij}s_{ij})^{1/2}, \quad \overline{\omega} = (2\omega_{ij}\omega_{ij})^{1/2}, \quad \tilde{s} = \max(\overline{s},\overline{\omega}) \quad .$$

Apsley and Leschziner (1998)

$$c_1 = \frac{(-a_{12}^*)}{\tilde{s}}\left[\frac{1+(\frac{1}{3}\beta^2\tilde{s}^2-\gamma^2\overline{\omega}^2)/\tilde{s}^2}{1+\frac{1}{3}\beta^2-\gamma^2}\right] \ ,$$

$$c_2 = \frac{6(a_{11}^*+a_{22}^*)}{\tilde{s}^2}, \quad c_3 = \frac{a_{11}^*-a_{22}^*}{\tilde{s}^2},$$

$$(c_5\ ,\ c_6) = (-\frac{6\gamma^2}{\tilde{s}^2}\ ,\ -\frac{6\beta\gamma}{\tilde{s}^2})\frac{(-a_{12}^*)}{\tilde{s}(1+\frac{1}{3}\beta^2-\gamma^2)} \quad ,$$

$$\overline{s} = (2s_{ij}s_{ij})^{1/2}, \quad \overline{\omega} = (2\omega_{ij}\omega_{ij})^{1/2},$$

$$\frac{1}{\tilde{s}} = \frac{2f_0}{\sigma^* + \sqrt{\sigma^{*2}+2f_0(f_0-1)(\tilde{s}^2+\overline{\omega}^2)}},$$

$$f_0 = 1+1.25\max(0.09\sigma^{*2},1), \quad \beta = 0.222, \quad \gamma = 0.623$$

a_{12}^*, a_{11}^*, a_{22}^* and σ^* are functions of y^*, based on DNS data for fully-developed channel flow. For large y^*, $(a_{12}^*, a_{11}^*, a_{22}^*, \sigma^*) = (-0.3, 1.0, 0.4, 3.33)$.

References

Apsley, D.D. and Leschziner, M.A., 1998, "A new low-Reynolds-number nonlinear two-equation turbulence model for complex flows", *Int. J. Heat Fluid Flow*, Vol. 19, pp. 209-222.

Bachalo, W.D. and Johnson, D.A., 1986, "Transonic, turbulent boundary-layer separation generated on an axisymmetric flow model", AIAA J., Vol. 24, pp. 437-443.

Craft, T.J., Launder, B.E. and Suga, K., 1996, "Development and application of a cubic eddy-viscosity model of turbulence", *Int. J. Heat Fluid Flow*, Vol. 17, pp.108-115.

Fleming, J.L., Simpson, R.L., Cowling, J.E. and Devenport, W.J., 1993, "An experimental study of a turbulent wing-body junction and wake flow", *Exp. Fluids*, Vol. 14, pp. 366-378.

Gatski, T.B. and Speziale, C.G., 1993, "On explicit algebraic stress models for complex turbulent flows", *J. Fluid Mech.*, Vol. 254, pp. 59-78.

Gibson, M.M. and Launder, B.E., 1978, "Ground effects on pressure fluctuations in the atmospheric boundary layer", *J. Fluid Mech.*, Vol. 86, pp. 491-511.

Hanjalic, K., Jakirlic, S. and Hadzic, I., 1997, "Expanding the limits of "equilibrium" second-moment turbulence closures", *Fluid Dynamics Research*, Vol. 20, pp. 25-41.

Jakirlic, S., and Hanjalic, K., 1995, "A second-moment closure for non-equilibrium and separating high- and low-Re-number flows", *Proceedings, 10th Symposium on Turbulent Shear Flows*, Penn.-State University, USA.

Obi, S., Aoki, K. and Masuda, S., 1993, "Experimental and computational study of turbulent separating flow in an asymmetric plane diffuser", *Proceedings, 9th Symposium on Turbulent Shear Flows*, Kyoto, Japan.

Shima, N., 1998, "Low-Reynolds-number second-moment closure without wall-reflection redistribution terms", *Int. J. Heat Fluid Flow*, Vol. 19, pp. 549-555.

Speziale, C.G., Sarkar, S. and Gatski, T.B., 1991, "Modelling the pressure-strain correlation of turbulence: an invariant dynamical systems approach", *J. Fluid Mech.*, Vol. 227, pp. 245-272.

Speziale, C.G. and Xu, X-H., 1996, "Towards the development of second-order closure models for nonequilibrium turbulent flows", *Int. J. Heat Fluid Flow*, Vol. 17, pp. 238-244.

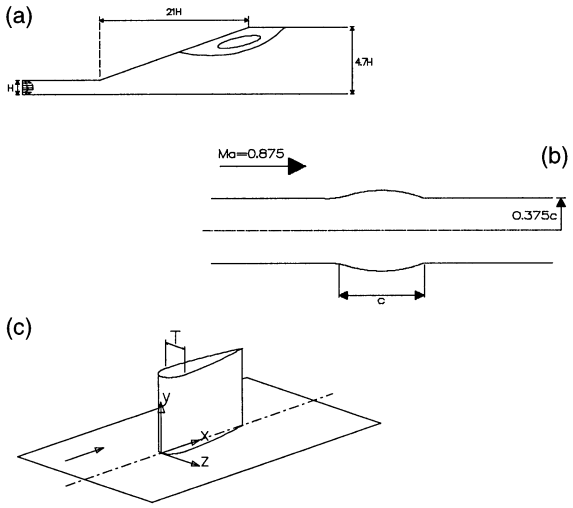

Figure 1. Geometry of test cases: (a) plane asymmetric diffuser; (b) transonic bump; (c) wing-body junction.

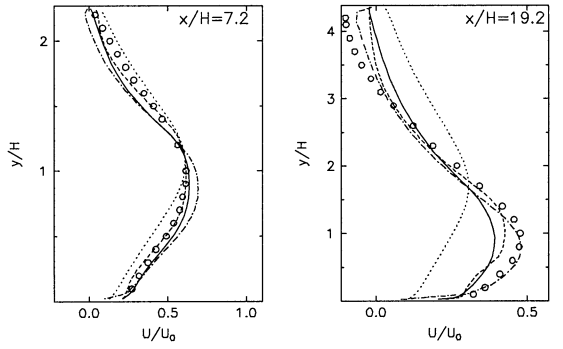

Figure 2. Diffuser: mean-velocity profiles with eddy-viscosity closures; o experiment, ... Launder and Sharma k-ε; — · — · — Gatski and Speziale; ----- Apsley and Leschziner; ——— Craft *et al.*

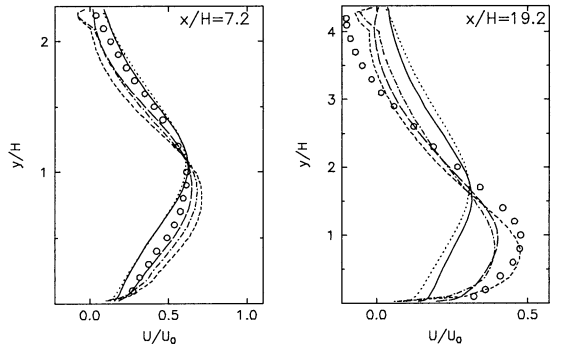

Figure 3. Diffuser: mean-velocity profiles with second-order closures; o experiment, ... Launder and Sharma k-ε; — · — · — Gibson and Launder; ----- Speziale *et al.*; — — — — Shima; ——— Jakirlic and Hanjalic.

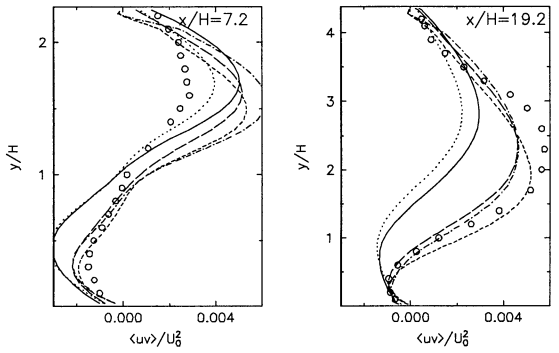

Figure 4. Diffuser: shear-stress with second-order closures; key as for Figure 3.

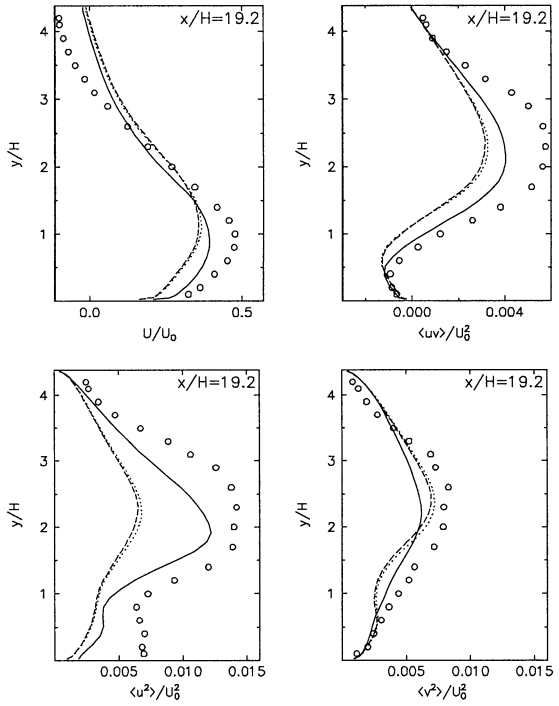

Figure 5. Diffuser: effect of non-linear terms in the Craft *et al.* NLEVM; o experiment; ——— full model; ----- quadratic terms omitted; ..... quadratic and curvature terms omitted.

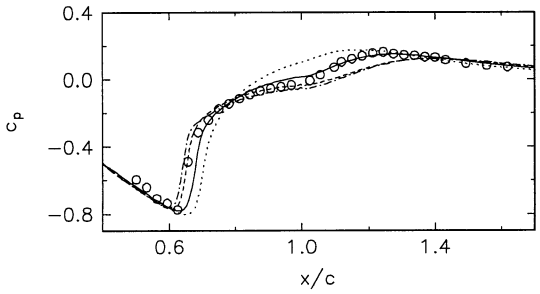

Figure 6. Transonic bump: surface pressure coefficient with eddy-viscosity closures; o experiment, ... Launder and Sharma k-ε; — · — · — Gatski and Speziale; ----- Apsley and Leschziner; ——— Craft *et al.*

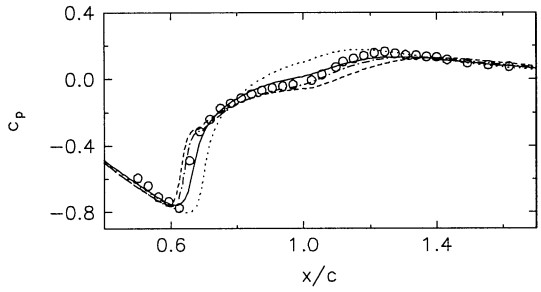

Figure 7. Transonic bump: surface pressure coefficient with differential stress closures; o experiment, ... Launder and Sharma k-ε; — · — · — Gibson and Launder; ----- Speziale *et al.*; ——— Jakirlic and Hanjalic.

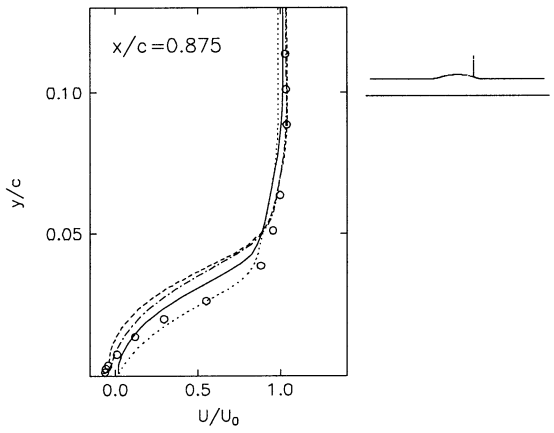

Figure 8. Transonic bump: mean-velocity profiles with second-order closures; key as Figure 7.

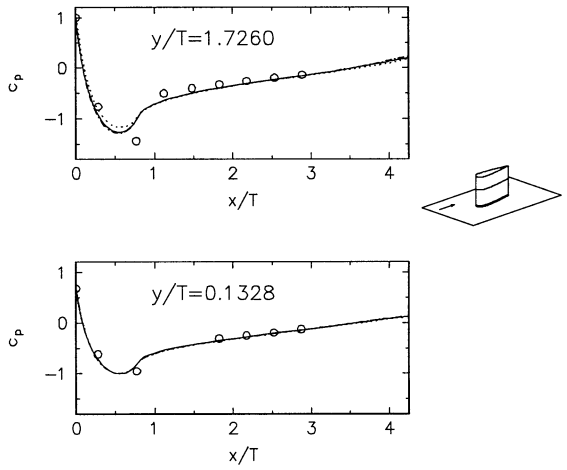

Figure 9. Surface-pressure coefficient on wing: o experiment, ... Launder and Sharma k-ε; — · — · — Apsley and Leschziner NLEVM; ——— Gibson and Launder DSM.

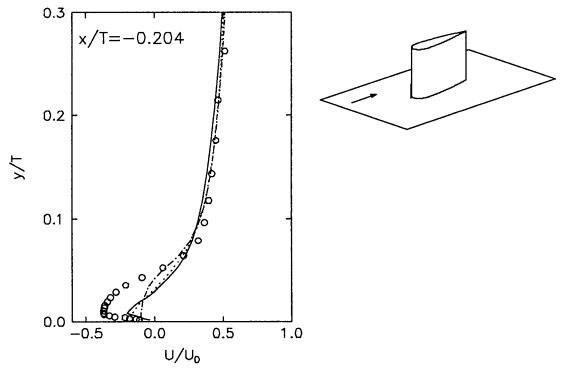

Figure 10. Streamwise mean-velocity profile in upstream vortex; key as for Figure 9.

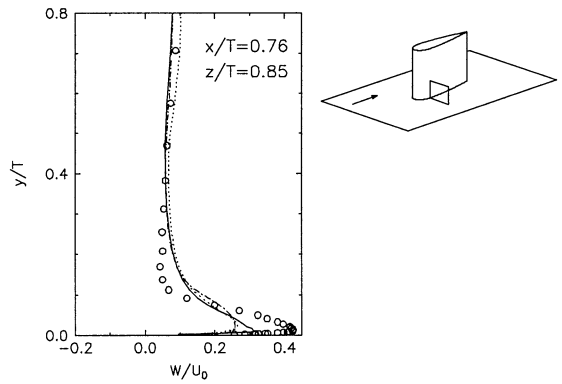

Figure 11. Secondary velocity profile in crosswind plane; key as for Figure 9.